ELSEVIER

Journal of Structural Geology 28 (2006) 1040–1050

JOURNAL OF STRUCTURAL GEOLOGY

www.elsevier.com/locate/jsg

Kinematic and dynamic fault slip analyses: implications from the surface rupture of the 1999 Chi-Chi, Taiwan, earthquake

Tom G. Blenkinsop

School of Earth Sciences, James Cook University, Townsville QLD 4811, Australia

Abstract

The 1999 Chi-Chi earthquake created a 100-km-long surface rupture on the Chelungpu thrust fault in Taiwan due to convergence between the Phillipine Sea and Eurasian plates. Fault slip measurements were made by several researchers from the entire length of the rupture directly following the earthquake and can thus be attributed to a single tectonic event. Conventional fault slip analyses are applied to these data and the results are compared with independent seismological and kinematic observations. Unlike many fault slip analyses, complications due to multiple deformations can be categorically excluded and the results can be evaluated from the seismological and plate movement data. Kinematic analyses of fault slip data that are weighted by displacement show sub-horizontal NW–SE shortening that is parallel to the plate convergence vector. A single fault plane solution satisfies almost all the data. Right dihedra and trihedra solutions also satisfy almost all the surface rupture measurements and give σ_1 in a NW–SE orientation that is similar to the results of stress inversion and to inversion from earthquakes in the Chi-Chi earthquake sequence. Despite criticisms of fault slip analysis methods, these results show that fault slip analyses from data collected along major faults, which have not witnessed multiple deformation events, can be valid. Homogeneous strain and stress states exist in the sense that kinematic and dynamic solutions can be found that fit essentially all the data, and these solutions have tectonic significance.

Keywords: Fault slip analysis; Kinematics; Dynamics; Paleostress; Earthquake

1. Introduction

Fault slip analyses attempt to derive kinematic or dynamic data from the orientations of fault planes and slip vectors (e.g. Angelier, 1994; Ramsay and Lisle, 2000). However, there has been considerable controversy over the validity of several proposed methods (e.g. Dupin et al., 1993; Pollard et al., 1993; Twiss and Unruh, 1998; Roberts and Ganas, 2000; Gapais et al., 2000) because of five potential problems:

(1) Fault slip data belonging to different deformation events may be difficult to separate.
(2) Faults may be reorientated during a single or multiple deformation events.
(3) Stress/strain/strain rate tensors in a single deformation event may not be homogeneous.
(4) The assumption made in several methods that fault slip occurs in the direction of maximum resolved shear stress (the 'Wallace–Bott' hypothesis; Wallace, 1951; Bott, 1959).
(5) Should fault slip data be analysed in terms of strain or strain rate (kinematic analysis) or in terms of stress (dynamic analysis)?

The first two problems are due to superimposed deformation events and are the subject of vigorous current research (e.g. Nemcok et al., 1999; Yamaji, 2000; Shan et al., 2003, 2004; Liesa and Lisle, 2004; Shan and Fry, 2005). Points 3 and 4 remain fundamental potential difficulties, but have received less attention recently. These two factors may be related and they may also be scale dependant.

The debate about how fault slip data should be treated (point 5) has been well summarised by Marrett and Allmendinger (1990), Twiss and Unruh (1998) and Gapais et al. (2000). Early fault slip analyses emphasised a dynamic approach (e.g. Carey and Brunier, 1974; Angelier, 1975; Etchecopar et al., 1981; Armijo et al., 1982) and 'paleostress analysis' has remained an important method in structural geology since then (e.g. Wojtal and Pershing, 1991; Angelier, 1994). However, the formation of faults has been increasingly viewed in kinematic terms over the last 30 years (e.g. Aydin and Reches, 1982; Reches, 1983; Krantz, 1988) and, as pointed out elegantly by Twiss and Unruh (1998), the fundamental significance of fault slip data is kinematic because an identifiable movement on a fault is a displacement, not a stress. Kinematic fault slip analyses are

E-mail address: Thomas.Blenkinsop@jcu.edu.au.

0191-8141/$ - see front matter © 2006 Elsevier Ltd. All rights reserved.
doi:10.1016/j.jsg.2006.03.011

Table 1
Methods of fault slip analysis

	Method	Result	Notes	Examples
Kinematic	Moment tensor summation (unweighted)	Principal incremental strains/strain rates, e_3 and e_1 (extension positive)	Assumes fault kinematics are scale invariant	Marrett and Allmendinger (1990)
	Moment tensor summation (weighted)	Principal incremental strains/strain rates, e_3 and e_1 (extension positive)	Requires displacement estimate for each fault	Marrett and Allmendinger (1990)
Dynamic	Right dihedra	Principal stress orientations, σ_1 and σ_3 (compression positive)	Slip vector in direction of resolved stress	Angelier and Mechler (1977)
	Right trihedra	Principal stress orientations, σ_1 and σ_3 (compression positive)	Slip vector in direction of resolved stress	Lisle (1987)
	Stress inversion	Principal stress orientations, σ_1 and σ_3 (compression positive)	Assumes slip in direction of maximum resolved shear stress	Angelier (1984); Gephart and Forsyth (1984)

directly comparable with seismological focal mechanism solutions (e.g. Marrett and Allmendinger, 1990). Twiss and Unruh (1998) argued that fault slip data can be considered in terms of incremental strain, or preferably strain rate, since strain rate is obtained by dividing strain by a scalar property, time, that does not affect the orientations or relative magnitudes of the principal values. Table 1 summarises some methods that can be used to treat fault slip data, and shows the results obtained from each method. Specific assumptions of the methods are also noted.

This study is based on the outstanding data collected following the 1999 Chi-Chi earthquake in Taiwan, which is one of the best ever documented earthquakes (Shin and Teng, 2001). Fault slip data are available from exposures of the 100-km-long earthquake rupture (e.g. Lee et al., 2003). The earthquake has also been comprehensively examined from the seismological point of view (Teng et al., 2001). The data collected from the Chi-Chi earthquake present a possibly unique opportunity to apply conventional fault slip analyses to a single seismic event on a large fault and to compare the results with seismological data. Analysis of a single slip event is an excellent test case for fault slip analyses, since all complications from multiple deformations are eliminated. A further justification for this approach is that possible violations of the Wallace–Bott hypothesis due to collection of data from the surface have been demonstrated by Pollard et al. (1993) to be "not much greater than field measurement errors or analysis imprecision".

2. Geological background

Taiwan is situated on a complex plate margin between the Phillipine Sea and Eurasian plates, which are converging at a rate of 82 mm/yr on an azimuth of 299° (Seno et al., 1993). To the northeast of Taiwan, the Phillipine Sea plate is being subducted under the Eurasian plate along the Ryuku trench; to the south of the island, the Eurasian plate is being subducted beneath the Phillipine Sea plate along the Manila trench (Fig. 1). Plate convergence is taken up in central Taiwan on a series of east-dipping thrust slices in the Taiwan fold-and-thrust belt.

The Mw 7.6 Chi-Chi earthquake of 20th September 1999 occurred on one of these thrusts, the Chelungpu fault, and produced a surface rupture 100 km long with an epicentre at 120.82° E, 23.85° N and a focal depth of 8 km (Shin and Teng, 2001). The rupture produced a fault scarp ranging from 1 m high at the southern end to 8 m at the northern end, due to reverse movement on the generally east-dipping fault plane. It was the largest on-land earthquake to occur in Taiwan in the last century, causing 2470 deaths and destroying more than 100,000 structures (Shin and Teng, 2001).

The earthquake ruptured northwards in a series of irregular sub-events or jumping dislocations (Kao and Chen, 2000) over a non-planar rupture surface with an inhomogeneous slip distribution (e.g. Wang et al., 2001). Slip around the hypocentre towards the south of the fault was small and increased towards the northern end of the fault. The southern end of the fault consists of a distinct NE-striking segment on which slip was right-lateral, compared with the mainly thrust sense of slip on the rest of the fault. At the northern end of the fault, the strike becomes E–W. The surface rupture propagation

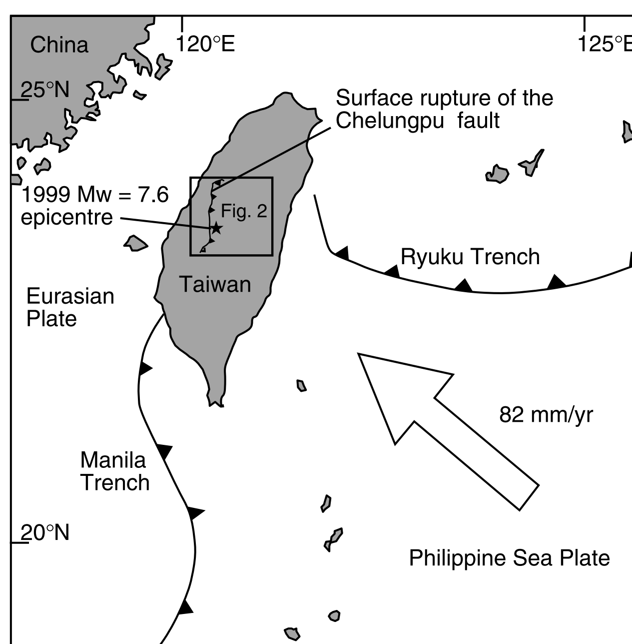

Fig. 1. Tectonics of Taiwan and the Chi-Chi earthquake. Large open arrow shows direction of plate convergence. After Lee et al. (2002).

was clearly influenced by pre-existing geological structures such as weaker shale layers and folds (Lee et al., 2002).

The Chi-Chi earthquake has provided more geophysical data than any other large earthquake. This was partly due to the completion shortly before the earthquake of a network of 650 strong motion instruments (which increased the total global records by five times alone) and ongoing GPS programs (Shin and Teng, 2001). Field surveys launched immediately after the earthquake along the 100 km surface rupture of the Chelungpu fault provided detailed records of the surface rupture (J.C. Lee et al., 2002; Y.H. Lee et al., 2003; Angelier et al., 2003a,b), which were used in this study.

3. Data and methods

The field surveys are regarded as data for a typical fault slip analysis, the results of which can be compared with the seismological inferences. The dip slip component of movement was reverse in all cases. Lee et al. (2002) made seven determinations of fault slip data from the northern part of the rupture by direct measurements of fault surfaces, striations and displaced markers. Lee et al. (2003) made similar types of observations at 97 stations along the whole length of the rupture, from which fault slip data could be derived for 85 stations. In many cases a range of values was given by Lee et al. (2003) for parameters such as fault azimuth, dip or slip: in these cases the average value was used in this study. Angelier et al. (2003a,b) provided data for two additional sites in the central part of the rupture by analysing displaced markers; one of the two sites included two sub-sites. A total of 94 data were thus assembled, comprising location, fault and slip orientation, and displacement (Fig. 2; Appendix A). These are referred to as the surface rupture data. They are distributed irregularly throughout the whole length of the rupture, perhaps analogous to the irregular distribution of sampling points in a fault slip analysis. In both a typical fault slip analysis and this study, the location of the sampling points is determined by available exposures of faults.

The data were subdivided into five areas, A–E, from north to south according to the division used in Lee et al. (2003), who noted distinct changes in fault plane orientations in these sub areas. The northern area, A, is characterised by S to SE dipping fault planes with down-dip slip vectors. The central areas, B–D, have easterly dipping fault planes with slip vectors that change systematically from left lateral, reverse oblique slip in B, to reverse slip in C and reverse-right lateral oblique slip in D. Area E has SE dipping fault planes with dominant right lateral movement.

The fault slip data were analysed both in aggregate and in each of the five area groups by conventional fault slip methods (Table 1). Moment tensor summations of P and T axes (both unweighted and weighted by measured displacement) as implemented in FaultKin 4.3 by Allmendinger et al. (http://www.geo.cornell.edu/geology/faculty/RWA/RWA.html) are reported using eigenvectors $E_1 \geqq E_2 \geqq E_3$ (extension positive). The assumptions and limitations of these methods are explained in the FaultKin manual and in Marrett and Allmendinger (1990). The right dihedra and trihedra methods were used for dynamic analysis (Angelier and Mechler, 1977; Lisle, 1987; Ramsay and Lisle, 2000). A grid search was also made for the best-fit stress tensor. Compressive stress is taken as

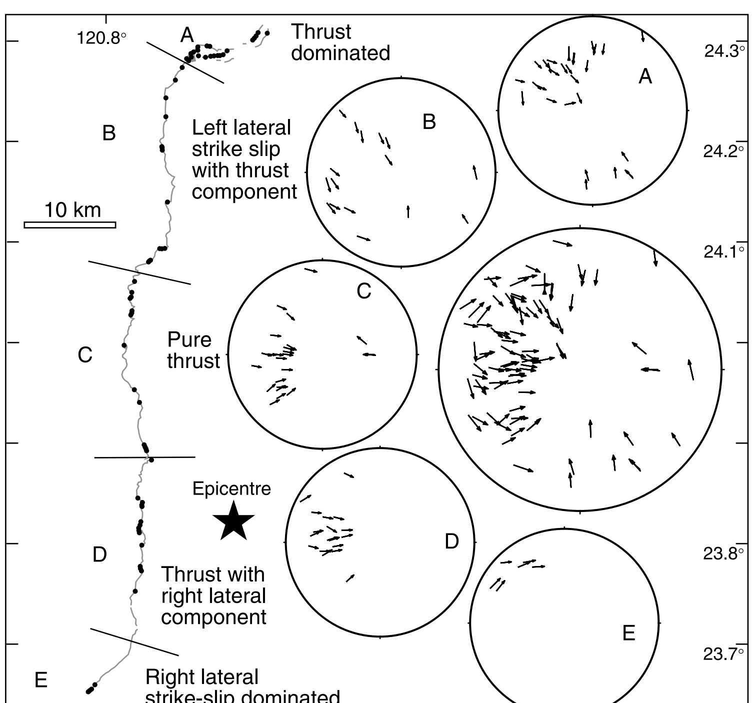

Fig. 2. Location of the measurement stations (dots) along the trace of the Chelungpu fault (grey line) and subdivision into areas from Lee et al. (2003). Large stereoplot shows tangent lineation diagram for the entire surface rupture data set, smaller plots show data from individual areas, using the convention that the arrow shows footwall movement. All stereoplots are lower hemisphere, equal area.

positive and the stress ratio Φ is $(\sigma_2-\sigma_3)/(\sigma_1-\sigma_3)$ (cf. Angelier, 1975). Complete grid searches (i.e. ranging from 0 to 359° azimuth and from 0 to 90° plunge) were conducted in angular increments of 1° and Φ increments of 0.05. Although these searches were very time consuming, attempts to start with a complete coarse search and proceed by finer partial searches, as recommended by Ramsay and Lisle (2000), did not succeed with these data because there appeared to be many metastable solutions. The quality of the result of the grid search is indicated by the deviation, which is the average angular difference between the calculated maximum resolved shear stress and the observed slip lineation. Although the deviation is not an ideal measure for the fit of the inversion (cf. Yamaji, 2003), it can be compared directly with results from seismological inversions (Kao and Angelier, 2001).

4. Results

4.1. Kinematic analyses

Moment tensor solutions are given in Table 2 and displayed in Fig. 3. Solutions for the moment tensors for whole data set (unweighted and weighted by displacement) can be compared with seismologically determined double couple centroid moment tensors (Table 2; Fig. 3). The solutions for the surface rupture data indicate a horizontal, NE–SW orientation for E_3 and a sub-vertical orientation for E_1. 97% of the P and T axes fall within the respective shortening and extensional quadrants of the fault plane solution from the surface rupture data (Fig. 3b). Unweighted and weighted moment tensors are also given for the five areas in Table 2 and the weighted tensors are shown in Fig. 4. There is considerable and systematic variation in the orientation of the eigenvectors along the fault plane. E_3 is

Table 2
Moment tensor solutions for the surface rupture data and from seismological results for the Chi-Chi earthquake. USGS—United States Geological Survey, national Earthquake Information Centre (http://wwwneic.cr.usgs.gov/) ERI—Earthquale Research Institute, University of Tokyo (http://www.eri.u-tokyo.ac.jp/index.html, Harvard—Harvard Centroid Moment Tensor catalogue (http://www.seismology.harvard)

Surface rupture data set	E_1		E_2		E_3	
	Trend	Plunge	Trend	Plunge	Trend	Plunge
Unweighted moment tensor	238	90	19	0	109	0
Weighted moment tensor	243	89	30	1	120	1
DoubleCouple CMT						
USGS	36	69	157	11	250	18
ERI	213	73	63	15	331	8
Harvard	116	70	212	2	303	20
Wu et al. (2001)	74	71	184	7	276	18
Areas						
Unweighted moment tensors						
A	241	88	60	2	150	0
B	200	67	37	23	302	5
C	143	87	1	3	271	2
D	352	79	179	11	89	1
E	7	35	188	55	97	1
Weighted moment tensors						
A	318	86	69	2	159	4
B	203	48	34	41	299	6
C	144	83	360	6	270	4
D	347	82	185	7	94	2
E	359	34	189	56	92	5

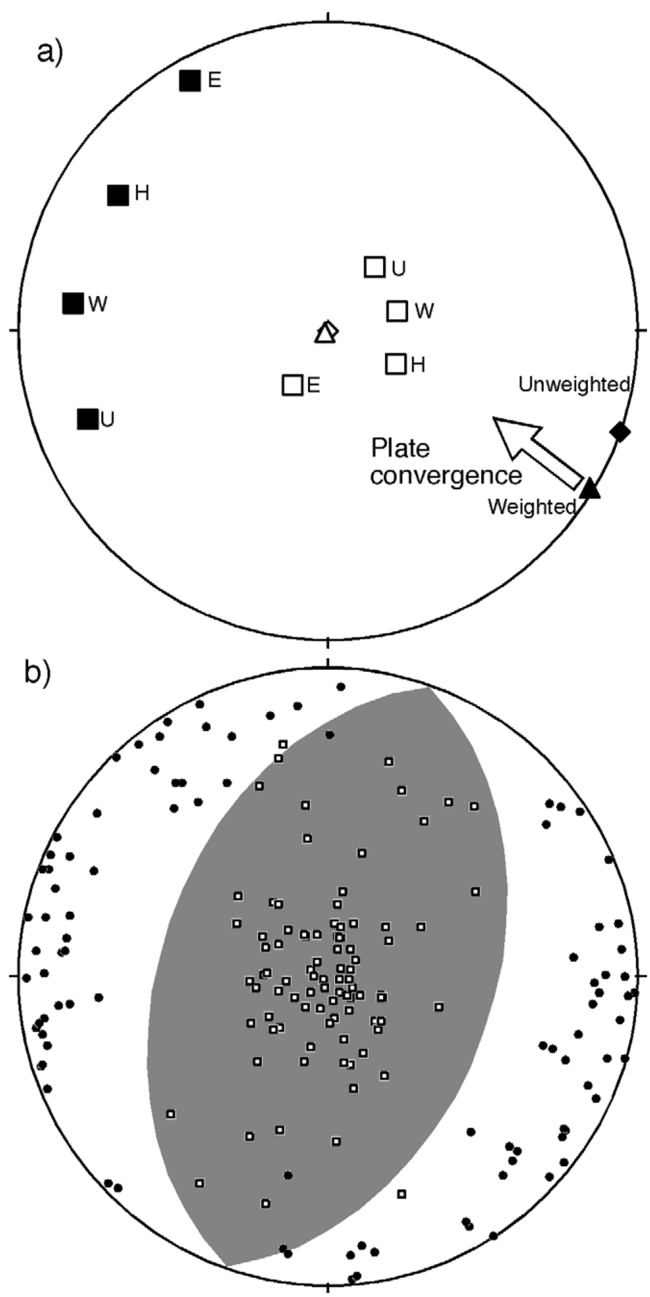

Fig. 3. (a) Moment tensor solutions for the entire surface rupture data set (triangles—weighted, diamonds—unweighted) compared with seismologically derived estimates (squares). Filled symbols are E_3, open symbols E_1. Abbreviations: E—Earthquake Research Institute, University of Tokyo, H—Harvard Centroid Moment Tensor catalogue, U—United States Geological Survey, W—Wu et al. (2001) (see Table 2 for www addresses). (b) P and T axes and fault plane solution for the weighted moment tensor of the surface rupture. Black circles are P axes, open squares are T axes, shaded area is the T quadrant.

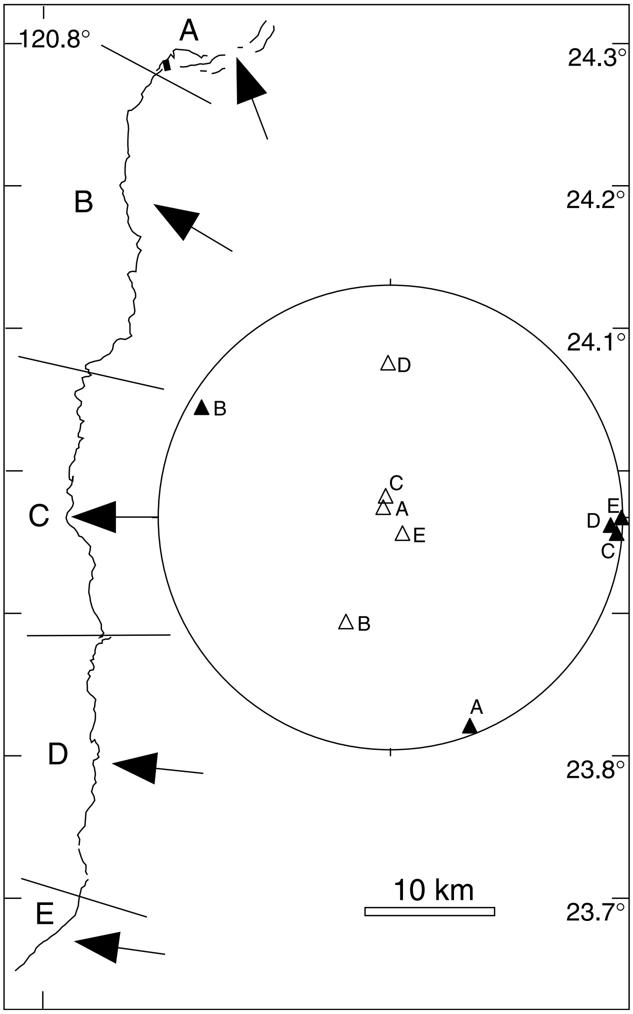

Fig. 4. Variation of weighted moment tensors along the Chelungpu fault. Arrow shows the azimuth of E_3 in each of the five areas. Filled triangles—E_3, open triangles—E_1.

E–W for the southern half of the fault and rotates clockwise over 50° to NNW–SSE in the northern part of the fault (Fig. 4).

4.2. Dynamic analyses

Right dihedra and trihedra solutions for the total data set are shown in Fig. 5. The right dihedra solution shows σ_1 sub-horizontal and trending ESE; this solution is compatible with 99% of the data (only one surface measurement does not fit this solution). The right trihedron solution gives a general region of high probability for σ_1 in the same direction, but the maximum probability suggests a sub-horizontal ENE orientation for σ_1. The results of the grid search for stress are shown in Table 3 (rows labelled Inversion) and the result for the entire data set displayed in Fig. 6, which also shows inversions obtained by Kao and Angelier (2001) from a dataset of 115 events in the Chi-Chi earthquake sequence, including one foreshock, from 20/9/1999 to 16/9/2000. Kao and Angelier (2001) analysed their data by progressively decreasing the largest misfit allowed in the inversion, reducing the number of events considered from 115 to 38 and yielding four results with

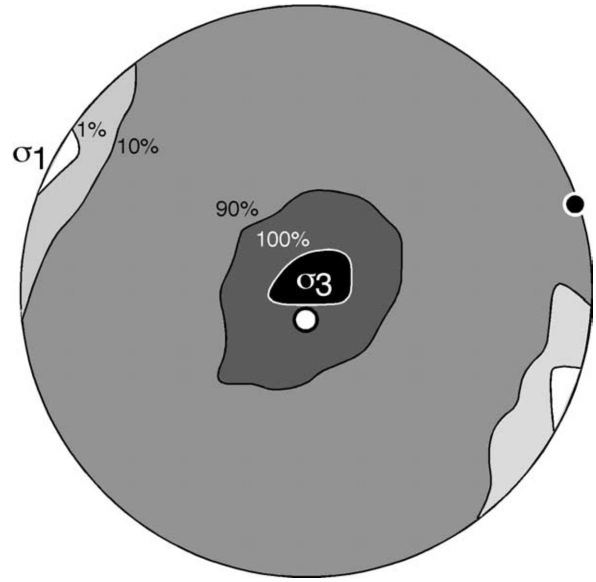

Fig. 5. Right dihedra and trihedra solutions for the entire surface rupture data set. The contours are the percentage of the faults whose σ_3 quadrants lie within the contour in the right dihedra method. The white spot indicates the optimum σ_3 from the right trihedra method: the probability of this direction as the σ_3 axis is 63%. The black spot is the most satisfactory σ_1 direction for this σ_3.

increasingly stringent fitting requirements, labelled 1–4 in Fig. 6. The surface rupture data show a sub-horizontal WNW orientation for σ_1 and a sub-vertical σ_3. The right dihedra and trihedra methods, and grid searches, were also applied to each of the five areas (Fig. 7). There is considerable variation in the orientation of the principal stress axes given by inversion within the sub-regions, from a NE-plunging orientation for σ_1 in the south, to W and WNW sub-horizontal in the central part, to a sub-horizontal NW–SE orientation in the northern part of the fault. The Φ values of the total data set and the aftershocks are all in the range 0.20–0.44, but the areas have very variable

Table 3
Dynamic analysis of the surface rupture data compared with stresses from seismological observations. Right dihedra, Inversion and Inversion: areas are solutions for the surface rupture data. Seismology are stresses obtained by Kao and Angelier (2001) from the earthquake sequence, using progressively more stringent requirements to obtaining a single tensor by discarding data that do not fit

	σ_1		σ_2		σ_3		ϕ	Dev
	Trend	Plunge	Trend	Plunge	Trend	Plunge		
Right dihedra	111	3			11	88		
Inversion								
	291	5	21	0	111	85	0.2	21
Seismology								
1	299	6	35	42	203	47	0.28	29
2	295	4	28	35	199	54	0.29	24
3	294	4	27	30	197	60	0.26	20
4	286	3	18	34	192	56	0.44	14
Inversion: areas								
A	145	12	54	4	307	77	0.2	13
B	135	3	44	25	232	65	0.9	15
C	97	12	6	3	260	78	0.55	7
D	294	9	200	18	50	70	0.15	7
E	44	32	300	22	182	50	0.85	4

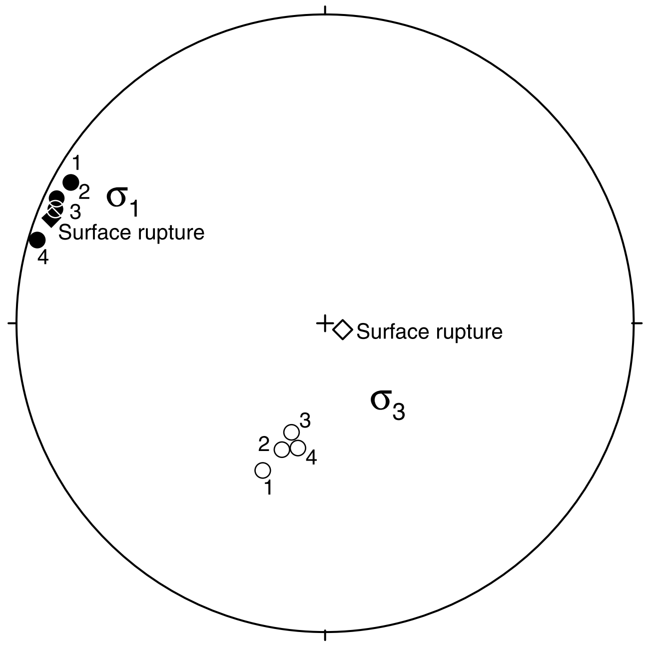

Fig. 6. Results of a grid search for stress from the entire surface rupture data (diamond symbols) compared with seismological results (circles) from the Chi-Chi earthquake sequence (Kao and Angelier, 2001). Filled symbols—σ_1, open symbols—σ_3. Numbers indicate the four increasingly stringent solutions from Kao and Angelier (2001).

Φ values, from 0.20 to 0.85, which do not vary systematically. The results of the right dihedra and trihedra methods agree closely with the inversions for the orientations of σ_3 in all areas except area E, and the methods also agree for the orientations of σ_1 in areas C and D. In area A, the right dihedra method and the inversions give similar orientations for σ_1, but the optimum σ_1 orientation for the right trihedra method trends southerly rather than SE in the other two methods. In area B, the right trihedra orientation for σ_1 is very similar to the inversion, but different from the right dihedra σ_1 orientation.

5. Discussion

5.1. Kinematic analyses

The moment tensors from the surface rupture data agree broadly with seismological results, indicating a NW–SE orientation for E_3 and a sub-vertical orientation for E_1, in accord with the known convergence between the Phillipine Sea and Eurasian plates. However, there is a consistent difference between the horizontal orientation of E_3 from the surface data and the WNW–NNW plunges of 8–20° in the seismological data. This can be related to the listric shape of the Chelungpu fault: the average surface dip is 52°, compared with the dips of 28–39° indicated from the seismological fault plane solutions. The tensors rotate from depth towards the surface with the fault plane.

There is an interesting difference between the weighted and unweighted moment tensors from the entire data set. The weighted orientation of E_3 is within 1° of the direction of convergence of the two plates, while the unweighted orientation is 10° anticlockwise.

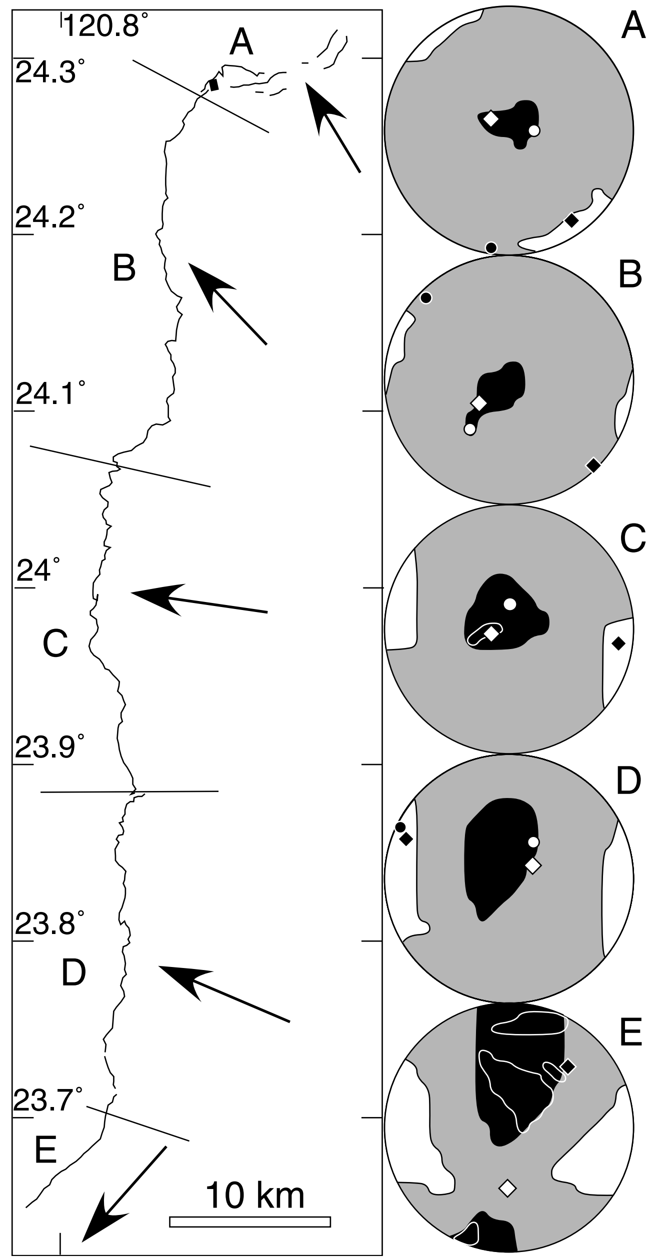

Fig. 7. Variation of stress along the Chelungpu fault from grid search (inversion) and right dihedra/trihedra methods. Arrows show the azimuth of σ_1 from the grid search in each of the five areas. Stereonets show the grid search results in diamond symbols (σ_1, black, σ_3, white). The right dihedra results are given by the contour fills (σ_1 white, σ_3, black). The right trihedra results are given by circle symbols in areas A, B and D. In these areas the right trihedra method identified a unique position for σ_3 (white circles) and the corresponding best fit σ_1 position is given by the black circles. In areas C and E, the white contour within the black area outlines the area for σ_3, and σ_1 lies in the white contour fill, as for the right dihedra method. The probabilities for σ_3 being in the directions shown in areas A–E are 71, 83, 88, 100 and 100%, respectively.

The regional variation in the tensors is very similar to that observed from coseismic displacements measured by GPS (Yu et al., 2001), as pointed out for the original surface rupture data by Lee et al. (2003). Inversions from near source strong motion records, broadband teleseismic data and GPS displacements amply demonstrate that this variation is caused by a clockwise rotation of the slip vector as the rupture propagated from south to north (Ma et al., 2001; Oglesby and Day, 2001; Zheng and Chen, 2001; Wang et al., 2001; Wu et al., 2001; Yoshioka, 2001).

The overwhelming majority of the P and T axes from the surface rupture are compatible with a single fault plane solution. Combined with the agreement of this solution with the known azimuth of convergence between the Phillipine Sea and Eurasian plates, these data suggest that a single kinematic tensor is valid for the surface rupture data, despite the regional variation, and that the tensor has a direct tectonic significance.

5.2. Dynamic solutions

The right dihedra solution and the stress inversion from the entire surface rupture data are similar, and also similar to the four solutions from the earthquake sequence, which describe the stress state well (Kao and Angelier, 2001). The shapes of the stress tensors are similar for the surface rupture and earthquake sequence and show that σ_2 is closer to σ_3 than to σ_1. The surface rupture data have an average deviation (21°) that is intermediate between the most and least stringent solutions provided by Kao and Angelier (2001). These observations suggest that a single stress tensor is valid for the vast majority of the surface rupture data when treated in aggregate and that it is the same tensor as inferred seismologically.

Individual stress tensors obtained from the areas A–E vary significantly in both orientation and stress ratios. σ_1 rotates clockwise from south to north (similar to the clockwise rotation of E_3). Kao and Angelier (2001) also noted this geographical variation and suggested that it was part of a fan-shaped pattern of stress trajectories characteristic of the whole collision zone. The discrepancies noted between the right dihedra and trihedra methods and the inversions reflect the different assumptions used in the methods, as discussed below, as well as a paucity of data in area E.

5.3. Implications for fault slip analyses

The kinematic and dynamic solutions for the data set of the surface rupture of the 1999 Taiwan earthquake demonstrate that fault slip analyses from large and representative enough data sets of single seismic events can be valid and have tectonic significance. The regional variation indicates that fault slip analyses from major structures should be made along as much of the structure as possible and that geographical variations in results may have geological explanations.

The above conclusions may also be valid for fault slip data collected from repeated ruptures that have similar geometries, including, but not necessarily limited to, characteristic earthquake behaviour. The better approximation of the weighted than unweighted moment tensors to the direction of plate convergence shows that displacement estimates should be collected and used in kinematic analyses (cf. Marrett and Allmendinger, 1990).

A significant difference between this study and many fault slip analyses is that the data used here were collected directly from the rupture of a major fault. Most fault slip analyses use data from small-scale faults (e.g. Lisle and Vandycke, 1996) that may be collected between major faults (e.g. Ghisetti, 2000). Analysing fault slip data from major ruptures separately from inter-fault data may have very important implications about the strength of major crustal faults (cf. Ghisetti, 2000).

The results reported here also bear on whether fault slip analyses should be kinematic or dynamic, or the different view that this dichotomy is false. The differences between the kinematic (Figs. 3 and 4) and dynamic analyses (Figs. 5–7) are anticipated consequences of the different methods used and *sui generis* do not distinguish which is more appropriate. The correspondence between the kinematic and dynamic solutions from the surface rupture data with independent data suggests that both approaches are valid for this data set. In this and other neotectonic studies, both approaches are useful because they can be compared with kinematic data from seismology and GPS studies, and dynamic data for stress inversions of earthquakes.

A practical drawback to kinematic analyses is the need to estimate fault slip magnitude for weighted solutions (Marrett and Allmendinger, 1990). On the other hand, because fault slip data are inherently kinematic, obtaining dynamic information from fault slip data may require additional assumptions (Twiss and Unruh, 1998), which need to be examined critically. In this regard, there is an important difference between dynamic methods concerning the assumption about the relation between the slip direction and the direction of maximum resolved shear stress. The stress inversion (grid search) methods assume the Wallace–Bott hypothesis that slip is in the direction of maximum resolved shear stress (e.g. Angelier, 1984), but, contrary to some accounts, the graphical right dihedra method does not make this assumption (cf. McKenzie, 1969; Table 1). The only assumption in the latter method is that slip occurs on the fault in the direction of some resolved shear stress. The right dihedra method is therefore a more general dynamic method, but provides no estimate of the stress ratio. The agreement between the inversions and the right dihedra/trihedra methods in this study suggests that the assumption of slip in the direction of maximum resolved stress is valid. If this validity is accepted, the extra information from the inversions (the relative magnitudes of the stresses) should also be reliable.

6. Conclusions

Surface rupture fault slip data from the 1999 Taiwan earthquake can be described very well by a single moment tensor, right dihedra/trihedra solutions and a single stress tensor. These results are obtained despite the highly complex nature of the rupture, which was influenced by local geological structures and occurred on a non-planar fault surface (e.g. Lee et al., 2002; Wang et al., 2001), and despite any fault interactions that occurred. Both the kinematic and dynamic analyses have a tectonic significance, as demonstrated by the correspondence of the solutions with independent analyses based on seismological and GPS measurements.

Both kinematic and dynamic solutions exhibit important regional variations. The kinematic data track the clockwise rotation of the slip vector during rupture propagation from north to south. The dynamic data can be related to a regional pattern of stress variation.

The single kinematic and dynamic solutions offer a tentative solution to the problem of strain/stress homogeneity in fault slip analyses. Although the data clearly have important heterogeneities, it is nevertheless possible to find single solutions that are valid for the vast majority of the data. Stress and strain can be considered homogeneous in as much as these solutions exist and have geological significance. Criteria for defining homogeneous stress and strain in this sense could be developed, such as a minimum proportion of P and T axes within appropriate quadrants, a minimum proportion of data in a right dihedron/trihedron solution, or a minimum angular misfit.

This seismological perspective suggests a cautiously favourable prognosis for fault slip analysis in the geological record. If enough data are collected in a representative way from large structures such as the Chelungpu fault, they can yield kinematic and dynamic solutions that have tectonic consequence. Furthermore, regional variations in strain or stress may be geologically significant, reflecting rupture complexity (kinematics) and regional variations in stress (dynamics). Although the validity of the fault slip analyses has only been demonstrated for active thrusting, there is no inherent reason why these results should not apply to other types of faulting.

Acknowledgements

Paul Evins contributed a useful appraisal of an early draft. The perceptive comments of the reviewers L. Arlegui and A. Yamaji, and the thorough editorial handling of R. Lisle, are greatly appreciated.

Appendix A

Fault slip data can be found in Table A1.

Table A1
Fault slip data. Sites 1–5 are from Lee et al. (2002). Sites labelled with letters A–E are from Lee et al. (2003). Site W: two estimates from Angelier et al. (2003a). Site K from Angelier et al. (2003b). All sites have been subdivided into the five groups recognised by Lee et al. (2003), from north to south. DipD is dip direction, Disp is displacement

Site	Longitude	Latitude	Fault plane			Slip vector		Sense	Disp
	(E)	(N)	Strike	Dip	DipD	Trend	Plunge		(m)
Area A									
5	120.876	24.302	10	65	E	180	20	T	1.44
A1	120.834	24.300	240	68	NW	307	66	T	5.45
A2	120.834	24.300	240	67	NW	305	64	T	5.50
A3	120.825	24.300	14	38	SE	111	37	T	1.35
A4	120.825	24.302	16	21	SE	77	18	T	2.20
A5	120.824	24.300	22	73	SE	94	72	T	5.85
A6	120.823	24.300	60	32	SE	134	31	T	1.90
A7	120.822	24.298	56	45	SE	149	45	T	1.05
A8	120.821	24.298	43	16	SE	158	15	T	2.85
4	120.815	24.290	235	50	NW	325	50	T	7.18
A9	120.790	24.284	60	43	SE	146	42	T	4.50
A10	120.790	24.274	250	60	NW	0	58	T	1.20
A11	120.787	24.281	45	48	SE	121	47	T	4.65
A12	120.782	24.281	100	56	S	188	56	T	5.85
A13	120.781	24.281	83	40	S	190	38	T	5.95
A14	120.778	24.280	70	49	SE	192	44	T	3.95
A15	120.775	24.280	92	55	S	197	54	T	4.25
A16	120.770	24.279	70	50	SE	190	45	T	2.00
A17	120.775	24.288	124	85	SW	134	63	T	3.80
A18	120.762	24.280	275	59	N	336	55	T	3.65
3	120.761	24.285	24	50	SE	115	50	T	1.96
A20	120.761	24.284	90	59	S	162	57	T	11.65
A21	120.753	14.282	68	57	SE	188	53	T	7.50
A22	120.753	24.282	24	55	SE	135	53	T	6.80
1a	120.752	24.282	40	65	SE	140	65	T	6.09
1b	120.752	24.282	50	58	SE	100	50	T	0.39
1c	120.752	24.282	45	60	SE	145	60	T	0.46
1d	120.752	24.282	45	55	SE	170	49	T	0.26
A24	120.752	24.279	275	68	N	349	67	T	3.80
Area B									
B1	120.749	24.276	216	73	NW	348	68	T	3.60
B2	120.747	24.274	330	60	NE	139	19	T	3.70
B4	120.745	24.271	42	47	SE	176	38	T	3.30

(*continued on next page*)

Table A1 (*continued*)

Site	Longitude	Latitude	Fault plane			Slip vector		Sense	Disp
	(E)	(N)	Strike	Dip	DipD	Trend	Plunge		(m)
B5	120.737	24.256	350	61	E	154	27	T	8.30
B6	120.728	24.238	350	68	E	167	9	T	7.45
B7	120.726	24.237	180	68	W	353	17	T	9.05
B8	120.727	24.175	333	69	NE	133	42	T	5.10
B9	120.726	24.175	333	73	NE	148	17	T	6.00
B10	120.725	24.176	300	70	NE	114	16	T	6.50
B11	120.731	24.134	44	15	SE	146	15	T	2.40
B12	120.717	24.088	65	28	SE	160	28	T	4.30
B13	120.723	24.088	45	57	SE	172	51	T	2.20
B14	120.728	24.088	45	77	SE	147	77	T	1.70
B17	120.713	24.079	60	35	SE	157	34	T	4.20
B18	120.713	24.079	360	60	E	142	47	T	3.40
B19	120.714	24.080	324	58	NE	124	28	T	3.00
B20	120.713	24.079	260	35	N	359	35	T	4.10
Area C									
C2	120.093	24.055	82	80	S	89	35	T	0.90
C3	120.690	24.045	328	44	NE	78	42	T	2.95
K1	120.691	24.044	321	46	NE	93	38	T	3.95
K2	120.691	24.044	321	48	NE	63	47	T	3.92
C5	120.690	24.041	50	44	SE	132	44	T	2.30
C7	120.670	24.042	49	56	SE	105	51	T	0.70
C8	120.690	24.025	360	46	E	96	45	T	4.90
C9	120.690	24.027	360	40	E	99	39	T	5.50
C10	120.688	24.020	360	50	E	108	49	T	2.80
W	120.688	24.020	4	30	E	101	30	T	3.27
C11	120.688	24.021	13	28	E	120	27	T	3.06
C12	120.688	24.021	360	31	E	98	30	T	2.80
C13	120.688	24.021	355	37	E	95	36	T	2.40
C16	120.682	23.982	22	45	SE	91	43	T	4.30
C18	120.705	23.978	180	41	W	270	41	T	0.90
C19	120.705	23.978	180	42	W	277	42	T	1.50
C20	120.694	23.947	160	37	W	313	19	T	0.70
C21	120.700	23.935	337	34	NE	95	31	T	1.20
C22	120.697	23.913	10	30	SE	105	30	T	0.00
C23	120.701	23.898	315	61	NE	72	58	T	1.20
C24	120.701	23.898	315	53	NE	65	51	T	1.30
C25	120.775	23.898	310	43	NE	53	42	T	1.55
C26	120.702	23.896	327	55	NE	45	54	T	1.70
C27	120.707	23.876	350	61	NE	110	57	T	1.85
Area D									
D1	120.702	23.833	356	61	E	112	58	T	4.55
D2	120.702	23.836	15	44	SE	122	43	T	6.80
D3	120.702	23.832	25	52	SE	96	50	T	5.70
D4	120.701	23.831	20	31	SE	87	29	T	3.20
D5	120.701	23.831	355	38	E	79	37	T	2.75
D6	120.702	23.828	351	50	E	89	50	T	4.85
D7	120.698	23.810	364	43	E	68	39	T	5.40
D8	120.698	23.810	364	41	E	70	38	T	5.95
D9	120.689	23.910	367	60	E	55	51	T	4.55
D10	120.698	23.808	349	39	E	78	39	T	1.95
D11	120.698	23.808	349	48	E	55	45	T	1.70
D12	120.698	23.807	310	42	NE	49	41	T	2.00
D13	120.701	23.794	65	68	SE	97	53	T	3.25
D14	120.701	23.777	30	82	SE	38	41	T	2.80
D16	120.701	23.777	30	43	SE	103	41	T	4.10
D17	120.700	23.770	10	57	SE	75	54	T	3.10
D18	120.700	23.770	10	30	SE	75	27	T	2.50
D19	120.695	23.749	25	64	SE	81	60	T	2.85
Area E									
E1	120.654	23.658	30	74	SE	37	23	T	2.15
E2	120.654	23.657	65	56	SE	80	21	T	0.95

Table A1 (*continued*)

Site	Longitude	Latitude	Fault plane			Slip vector		Sense	Disp
	(E)	(N)	Strike	Dip	DipD	Trend	Plunge		(m)
E3	120.652	23.656	30	68	SE	35	12	T	2.20
E4	120.651	23.654	46	79	SE	60	51	T	2.41
E5	120.649	23.652	55	65	SE	62	14	T	2.00
E6	120.648	23.652	60	65	SE	72	23	T	1.20

References

Angelier, J., 1975. Sur l'analyse de mesures recueillies sans des sites faillés: l'utilité d'une confrontation entre les méthodes dynamiques et cinématiques. Comptes Rendus de l'Académe des Sciences, Paris D281, 1805–1808.

Angelier, J., 1994. Fault slip analysis and palaeostress construction. In: Hancock, P.L. (Ed.), Continental Deformation. Pergamon Press, London, pp. 53–100.

Angelier, J., Mechler, P., 1977. Sur une méthode graphique de recherche des contraintes principales également utilisable en tectonique et en séismologie: la méthode des dièdres droits. Bulletin de la Societé Géologique de France 7, 1309–1318.

Angelier, J., Lee, J.-C., Chu, H.-T., Hu, J.-C., 2003a. Reconstruction of fault slip of the September 21st 1999, Taiwan earthquake in the asphalted surface of a car park, and co-seismic slip partitioning. Journal of Structural Geology 25, 345–350.

Angelier, J., Lee, J.-C., Chu, H.-T., Hu, J.-C., Chu, H.-T., 2003b. Three-dimensional deformation along the rupture trace of the September 21st 1999, Taiwan earthquake: a case study in the Kuangfu school. Journal of Structural Geology 25, 351–370.

Armijo, R., Carey, E., Cisternas, A., 1982. The inverse problem in microtectonics and the separation of tectonic phases. Tectonophysics 82, 145–160.

Aydin, A., Reches, Z., 1982. Number and orientation of fault sets in the field and in experiments. Geology 10, 107–112.

Bott, M.H.P., 1959. The mechanics of oblique slip faulting. Geological Magazine 96, 109–117.

Carey, M.E., Brunier, M.B., 1974. Analyse theorique et numerique d'un modele mecanique elementaire applique a l'étude d'une population de failes. Compte Rendus Hebdomadaires des Seances de l'Academie des Sciences 279, 891–894.

Dupin, J.M., Sassi, W., Angelier, J., 1993. Homogeneous stress hypothesis and actual fault slip: a distinct element analysis. Journal of Structural Geology 15, 1033–1043.

Etchecopar, A., Vasseur, G., Daignieres, M., 1981. An inverse problem in microtectonics for the determination of stress tensors from fault striation analysis. Journal of Structural Geology 3, 51–65.

Gapais, D., Cobbold, P.R., Bourgeois, O., Rouby, D., de Urreiztieta, M., 2000. Tectonic significance of fault-slip data. Journal of Structural Geology 22, 881–888.

Ghisetti, F., 2000. Slip partitioning and deformation cycles close to major faults in southern California: evidence from small-scale faults. Tectonics 19, 25–43.

Kao, H., Angelier, J., 2001. Stress tensor inversion for the Chi-Chi earthquake sequence and its implications on regional collision. Bulletin of the Seismological Society of America 91, 1028–1040.

Kao, H., Chen, W.-P., 2000. The Chi-Chi earthquake sequence: active out-of-sequence thrust faulting in Taiwan. Science 288, 2346–2349.

Krantz, R.W., 1988. Multiple fault sets and three-dimensional strain: theory and application. Journal of Structural Geology 10, 225–237.

Lee, J.C., Chu, H.-T., Angelier, J., Chan, Y.-C., Hu, J.-C., Lu, C.-Y., Rau, R.-J., 2002. Geometry and structure of northern surface ruptures of the 1999 Mw = 7.6 Chi-Chi Taiwan earthquake: influence from inherited fold belt structures. Journal of Structural Geology 24, 173–192.

Lee, Y.H., Hsieh, M.-L., Lu, S.-D., Shih, T.-S., Wu, W.-Y., Sugiyama, Y., Azuma, T., Kariyae, Y., 2003. Slip vectors of the surface rupture of the 1999 Chi-Chi earthquake, western Taiwan. Journal of Structural Geology 25, 1917–1931.

Liesa, C.L., Lisle, R.J., 2004. Reliability of methods to separate stress tensors from heterogenous fault-slip data. Journal of Structural Geology 26, 559–572.

Lisle, R.J., 1987. Principal stress orientations from faults: an additional constraint. Annales Tectonicae 1, 155–158.

Lisle, R.J., Vandycke, S., 1996. Separation of multiple stress events by fault striation analysis: an example from Variscan and younger structures at Ogmore, South Wales. Journal of the Geological Society, London 153, 945–953.

Ma, K.F., Mori, J., Lee, S.J., Yu, S.B., 2001. Spatial and temporal distribution of the slip for the 1999 Chi-Chi earthquake. Bulletin of Seismological Society of America 91, 1068–1087.

Marrett, R., Allmendinger, R.W., 1990. Kinematic analysis of fault-slip data. Journal of Structural Geology 12, 973–986.

McKenzie, D.P., 1969. The relation between fluid injection, plane solutions for earthquakes and the directions of principal stresses. Bulletin of Seismological Society of America 59, 591–601.

Nemcok, M., Kovac, D., Lisle, R.J., 1999. Stress inversion procedure for polyphase calcite twin and fault/slip data sets. Journal of Structural Geology 21, 597–611.

Oglesby, D.D., Day, S.M., 2001. Fault geometry and dynamics of the 1999 Ch-Chi (Taiwan) Earthquake. Bulletin of Seismological Society of America 91, 1099–1111.

Pollard, D.D., Saltzer, S.D., Rubin, A.M., 1993. Stress inversion methods; are they based on faulty assumptions? Journal of Structural Geology 15, 1045–1054.

Reches, Z., 1983. Faulting of rocks in three-dimensional strain fields—theoretical analysis. Tectonophysics 95, 133–156.

Ramsay, J.G., Lisle, R.J., 2000. The Techniques of Modern Structural Geology. Volume 3: Applications of Continuum Mechanics in Structural Geology. Academic Press, London.

Roberts, G.P., Ganas, A., 2000. Fault-slip direction in central and southern Greece measured from striated and corrugated fault planes: comparison with focal mechanism and geodetic data. Journal of Geophysical Research 105 (B10), 23443–23462.

Seno, T., Stein, S., Gripp, A.E., 1993. A model for the motion of the Phillipine Sea plate consistent with NUVEL-1 and geological data. Journal of Geophysical Research 98, 17941–17948.

Shan, Y., Fry, N., 2005. A hierarchical cluster approach for forward separation of heterogeneous fault/slip data into subsets. Journal of Structural Geology 27, 929–936.

Shan, Y., Suen, H., Lin, G., 2003. Separation of polyphase fault/slip data: an objective-function algorithm based on hard division. Journal of Structural Geology 25, 829–840.

Shan, Y., Li, Z., Lin, G., 2004. A stress inversion procedure for automatic recognition of polyphase fault/slip data sets. Journal of Structural Geology 26, 919–925.

Shin, T.-C., Teng, T.-L., 2001. An overview of the 1999 Chi-Chi, Taiwan, earthquake. Bulletin of Seismological Society of America 91, 895–913.

Teng, T.-l., Tsai, Y.-B., Lee, W. (eds.), 2001. Dedicated Issue on the Chi-Chi, Taiwan Earthquake of 20th September 1999. Bulletin of the Seismological Society of America 91, 893–1395.

Twiss, R.J., Unruh, J.R., 1998. Analysis of fault slip inversions; do they constrain stress or strain rate? Journal of Geophysical Research 103 (B6), 12205–12222.

Wallace, R.E., 1951. Geometry of shearing stress and relation to faulting. Journal of Geology 59, 118–130.

Wang, W.-H., Chang, S.-H., Chen, C.-H., 2001. Fault slip inverted from surface displacements during the 1999 Chi-Chi Taiwan, Earthquake. Bulletin of Seismological Society of America 91, 1167–1181.

Wojtal, S., Pershing, J., 1991. Paleostress associated faults of large offsets. Journal of Structural Geology 13, 49–62.

Wu, C., Takeo, M., Ide, S., 2001. Source processes of the Chi-Chi earthquake: a joint inversion of strong motion data with a multi-fault model. Bulletin of Seismological Society of America 91, 1128–1143.

Yamaji, A., 2000. The multiple inverse method: a new technique to separate stresses from heterogeneous fault-slip data. Journal of Structural Geology 22, 441–452.

Yamaji, A., 2003. Are the solutions of stress inversion correct? Visualization of their reliability and the separation of stresses from heterogeneous fault-slip data. Journal of Structural Geology 25, 241–252.

Yoshioka, S., 2001. Coseismic slip distribution of the 1999 Chi-Chi, Taiwan, earthquake deduced from inversion analysis of GPS data. Bulletin of Seismological Society of America 91, 1182–1189.

Yu, S.B., Kuo, L.C., Hsu, Y.J., Su, H.H., Liu, C.C., Hou, C.S., Lee, J.F., Lai, T.C., Liu, C.C., Liu, C.L., Tseng, T.F., Tsai, C.S., Shin, T.C., 2001. Preseismic deformation and coseismic displacements associated with the 1999 Chi-Chi, Taiwan earthquake. Bulletin of Seismological Society of America 91, 995–1012.

Zheng, Y., Chen, C.-H., 2001. Fault rupture processes of the 20th September 1999 Chi-Chi, Taiwan, Earthquake. Bulletin of Seismological Society of America 91, 1088–1098.